Comparison of fast three-dimensional simulation and actinic inspection for extreme ultraviolet masks with buried defects and absorber features

Chris H. Clifford,[a] Sandy Wiraatmadja, Tina T. Chan, and Andrew R. Neureuther
Department of Electrical Engineering and Computer Sciences, Cory Hall, University of California, Berkeley, California 94720

Kenneth A. Goldberg and Iacopo Mochi
Lawrence Berkeley National Laboratory, 1 Cyclotron Road, Berkeley, CA 94720

Ted Liang
Intel Corp., 2200 Mission College Blvd., Santa Clara, California 95054

(Received 13 July 2009; accepted 14 September 2009; published 3 December 2009)

The printability of buried extreme ultraviolet (EUV) defects near absorber features is studied using aerial images from the actinic inspection tool (AIT) and the fast EUV mask simulation program RADICAL. This work begins by comparing the printability of isolated defects through focus predicted by RADICAL and measured by the AIT. Then, images of defects near features from both simulation and experiment are investigated for different defect sizes and positions through focus. Finally, RADICAL is used to assess the expected defect printability levels in the less in coherent conditions which are expected to be used for production. Defect printability will be investigated as a function of defect size, position, and focus for the small absorber lines critical to 22 nm imaging using a top-hat illumination condition of sigma=0.75. Here, defects as small as 0.8 nm surface height cause a critical dimension (CD) change greater than 10% at best focus when located in the worst case position. Defects as small as 2.2 nm cause a CD change greater than 10% even when located under the center of the absorber. © *2009 American Vacuum Society.*
[DOI: 10.1116/1.3244624]

I. INTRODUCTION

Extreme ultraviolet (EUV) lithography is the leading contender to replace deep ultraviolet lithography for high volume semiconductor manufacturing, but there are still several roadblocks preventing its adoption. A major roadblock currently is the availability of defect free masks along with the necessary mask inspection and review infrastructure.[1] This work helps addresses the infrastructure issue by comparing the results of the fast EUV mask simulator RADICAL (rapid absorber defect interaction computation for advanced lithography) with experimental results from the actinic inspection tool (AIT) at Lawrence Berkeley National Laboratory (LBNL). These comparisons will help characterize and validate both tools as well as give insight into buried defect printability in EUV lithography.

First, images of isolated defects through focus at nearly coherent illumination are used to determine the aberrations in the AIT and validate the multilayer defect model used in RADICAL. Then, AIT images of defects near features are analyzed and compared to RADICAL simulations to determine the effect of defect size, defect position, and defocus on printability. Finally, RADICAL is used to predict the expected defect printability in advance for 22 nm line space patterns in production conditions with less coherent illumination.

II. BACKGROUND

An example sideview of an EUV mask with a buried defect and the resulting simulated aerial image is shown in Fig. 1. Without the defect, this mask would produce a line space pattern. But, as the aerial image in Fig. 1 shows, the defect causes a large disruption in the line.

A. AIT

In assessing the RADICAL simulation accuracy, we have been fortunate to have access to aerial image data from a programed defect mask measured on the AIT developed at LBNL.[2] The AIT is a direct charge-coupled device actinic (EUV-wavelength) EUV mask inspection tool. Recently the performance of the AIT was improved greatly and the data from December 2008 is nearly aberration-free compared to the data from August 2007. Both sets of data are used in this work. Fortunately the data on defect feature interactions are nearly aberration-free and can be compared to simulations without aberrations.

Bitmap aerial images recorded by the AIT are suitable for direct comparison with bitmaps from simulation. All simulations of AIT conditions in this work will assume a sigma of 0.1 and no magnification. For the isolated defect simulations done in 2007, the numerical aperture (NA) is 0.0625. For the 2008 simulations, the NA is 0.075. These values correspond to NA values of 0.25 and 0.3, respectively for a 4× system. Also, AIT focus values in this article represent the mask

[a]Electronic mail: chris@eecs.berkeley.edu

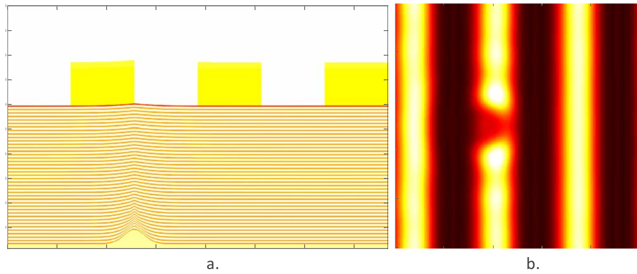

FIG. 1. (Color online) (a) Computer generated sideview of an EUV mask with a buried defect. (b) Resulting aerial image.

position. The Rayleigh defocus in this 1× system are 1.73 and 1.2 μm for NAs of 0.0625 and 0.075, respectively.

B. RADICAL

A new simulator, RADICAL, can simulate EUV masks with buried defects and absorber features three orders of magnitude faster than the finite difference time domain using two orders of magnitude less memory.[3] This speedup is accomplished by simulating the absorber features and defective multilayer separately using simulation methods optimized for each. This modularity makes the fast and accurate simulation of a large mask area containing buried defects possible.

C. Programed Defect Mask

All AIT inspections were done on the same programed defect mask (PDM) in which 48 nm high posts with a square base on a substrate are overcoated with a multilayer. The width of the posts is varied. It turns out that overcoating produced defects which all have between 50 and 60 nm full width at half maximum (FWHM) diameter and heights ranging up to 8 nm.[4] It has been shown previously by simulation that the most critical dimension (CD) of an overcoated buried defect is the surface height.[5] Therefore, the surface height will be the dimension used to characterize defect printability in this work. The substrate and surface sizes of all the defects on the mask are given in Table I. This mask contains areas of isolated defects as well as defects near dense absorber lines.

TABLE I. Summary of defect sizes on the programmed defect mask. All dimensions in nm.

Buried width	Buried height	Surface width (FWHM)	Surface height
100	48	60	8
95	48	59	7
90	48	58	6.2
85	48	56	5.3
80	48	55	4.4
75	48	54	3.5
70	48	53	2.6
65	48	52	1.7
60	48	51	0.8

III. COMPARISON OF IMAGES FROM AIT AND RADICAL

Isolated defects are considered first as a means of understanding the amplitude-phase nature of buried defects and tuning the model of the early AIT optical system. The comparisons of defects near features will then be used to give insight into buried defect printability for patterned masks.

A. Isolated buried defects

A detailed understanding of buried defects and the AIT imaging system can be extracted from the image of an isolated defect through focus. Figure 2 shows the center intensity of an isolated defect aerial image through focus from the AIT, recorded in 2007, and RADICAL. A novel method was

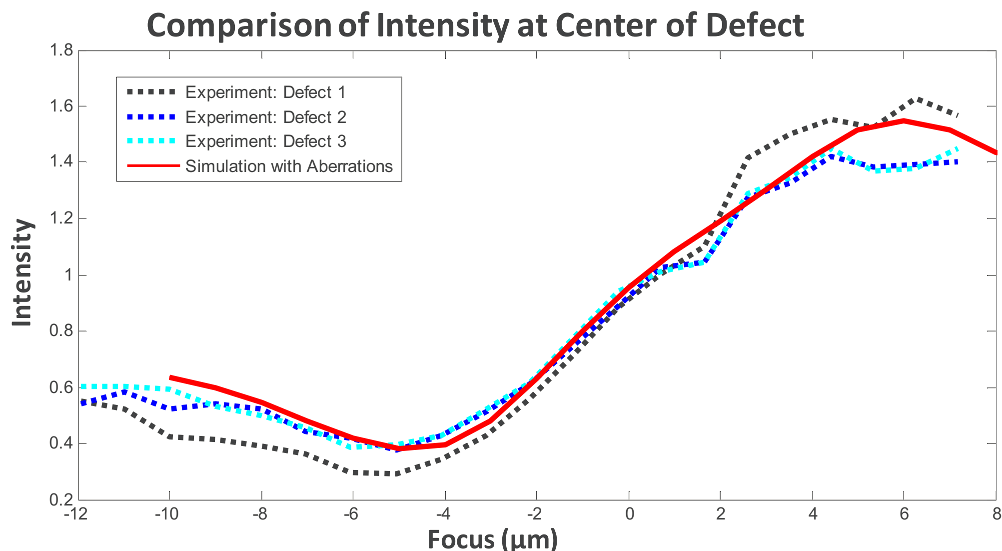

FIG. 2. (Color online) Center intensity value of aerial images of isolated defect from AIT experiments and RADICAL simulations.

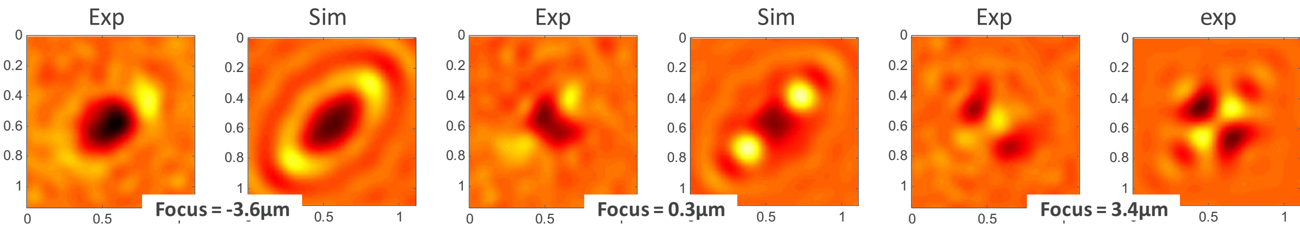

FIG. 3. (Color online) Comparison of experimental AIT images (labeled Exp) and simulated RADICAL images (labeled Sim) for three mask focus positions.

used to extract the aberrations present in the AIT in 2007.[6] When these aberrations are included, RADICAL matches the AIT data. A few example images of isolated defects at different focus positions are shown in Fig. 3. These images show that the RADICAL simulation predicts the correct image shape. This means that both the simulated electromagnetic defect response and imaging model are correct. The same through focus analysis was done with isolated defect images recorded on the AIT in 2008, and an optical model without aberrations matched the AIT data.[6] Therefore, for the rest of this work, the AIT data will be compared to RADICAL simulations without aberrations.

B. Buried defects near features

While isolated defects give insight into the nature of buried defects and the properties of an imaging system, defects near feature are what hinder the implementation of EUV lithography. In this section, several issues related to defects near features are investigated with images from AIT experiments and RADICAL simulations. First, the minimum sized defect causing a detectable CD change is determined. Then, the printability of covered defects in analyzed. Finally, the effects of the defect through focus are discussed. In this work, all reference to CD refers to the space CD. The space CD is the width of the bright areas of the image, corresponding to the space on the EUV mask between the absorber lines.

1. Minimum detectable defect size

Figure 4 shows the aerial images of five defects near dense lines recorded by the AIT. It is clear that the larger defects cause a more significant disruption than the smaller defects. In Fig. 4, the far right image, the 0.4 nm defect appears to have no effect on the aerial image. But, a quantitative analysis of the line width in the image shows that it does have a small effect. The standard deviation of the space CD in the images in Fig. 4 is 5.4 nm. But, near the defect in the 0.4 nm tall defect image the CD is consistently above the 3σ CD change of 16.2 nm, confirming that the AIT has the signal-to-noise ratio necessary to detect this 0.4 nm near a feature.

This is an encouraging and discouraging result. It is encouraging because it suggests that the AIT can detect subnanometer tall bump defects on EUV masks near features. But it is discouraging because even a defect as short as 0.4 nm on the multilayer surface is printable near a feature.

2. Printability of covered defects

The previous data were for defects centered between absorber lines, but the AIT data show that defects centered under the absorber can print as well. Figure 5 shows the layout, AIT image, and RADICAL image for a defect with a surface height of 7 nm centered under the absorber. The maximum CD change near the defect in the AIT image was 23 nm. A RADICAL simulation of the same geometry predicts a change of 19 nm.

It might be surprising that this defect causes a measurable CD change, but closer analysis shows that there is a physical reason. Although the center of the defect is covered, the Gaussian tail of the surface defect causes its disruption of the surface to extend into the space. The smoothing model in Ref. 7 predicts that the height of the defect at the edge of the absorber line is 2.2 nm, which corresponds to 0.33λ, round trip optical path length difference. This is a large percentage of a wavelength. That a phase difference of this magnitude affects the aerial image is not a surprise. The printability of buried defects under features will be covered more in Sec. V.

3. Effect of focus on defect printability

The light reflected from a buried defect in an EUV mask is out of phase with the background reflection. This results in an inversion of the center intensity of the aerial image of an isolated defect through focus, as shown in Fig. 2. This inversion in intensity is also apparent in the effect of a defect near

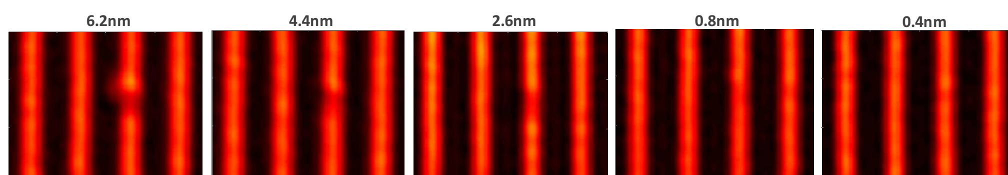

FIG. 4. (Color online) Experimental AIT images of buried defects of various sizes, surface height is labeled, centered in the reflecting area 60 nm away from the left edge of the absorber. The lines and spaces are each 250 nm.

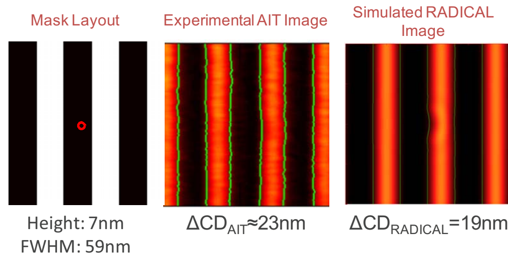

FIG. 5. (Color online) Layout, experimental image, and simulated image of a 7 nm tall, 59 nm wide defect centered under the absorber 43 nm away from the edge. The circle in the layout shows the position and half-max area of the defect on the surface.

a feature, as shown in Fig. 6. For negative focus, the defect causes the dark line to protrude into the space, for positive focus the space protrudes into the line. Near best focus, the defect has little effect indicating that measurements at several focal positions will likely be necessary in any mask inspection approach.

The images in Fig. 6 show a good qualitative match between RADICAL and the AIT images. This is an encouraging result because a through focus match requires a robust model of the defect feature interaction as well as the correct representation of the phase nature of the buried defect.

IV. PRINTABILITY STUDY FOR PRODUCTION EUV LITHOGRAPHY

RADICAL will now be used in advance of availability of high volume manufacturing quality exposure tools, resists, and masks to assess the expected defect printability levels in less coherent, production conditions. In this work, it is assumed that a defect causing 10% or larger change in CD is unacceptable. All simulations will be for 22 nm dense line space patterns. This will be referred to as the 22 nm node in the work, but the exact definition of the 22 nm node will vary with every semiconductor manufacturer. Also, the pitch for logic and memory are very different for a given node.

TABLE II. Summary of buried defect sizes and resulting surface defect sizes used in 22 nm node RADICAL simulations. All buried defects were rotationally symmetric Gaussian shaped. Widths are full width at half maximum.

Buried height	Buried width	Surface height	Surface width
2.5	50	0.8	74
5	50	1.4	73
10	50	2.2	71
15	50	2.8	71

A. Simulation conditions

The model assumed a prototypical EUV scanner for the 22 nm node is a 4× system with NA of 0.32. This corresponds to a $k1$ of about 0.5. Here either top-hat or annular illumination might be used. To emphasize the need for a high collection illuminator efficiency, a top-hat illumination system with sigma of 0.75 has been chosen for this work. The results will change if off-axis illuminations, like annular or dipole, are used. In fact, the improved image slope from these methods could reduce the effect of defects and increase defect tolerance and this deserves further study, but will not be investigated here.

The 13.5 nm light is incident on the mask at an angle of 6°. This incident light is perpendicular to the line space patterns simulated, causing shadowing and other effects on the final image.

CD is calculated with a constant threshold resist model. The threshold was chosen as the value that gives the nominal CD, in this case 22 nm, at best focus with no defect present. The size and position of the buried defect relative to the 88 nm dense lines on the mask will be varied. A summary of the buried defect sizes and shapes, along with the resulting surface defect sizes, is given in Table II.

B. Effect of position on printability

Figure 7 shows the range of defect positions simulated. A large offset range was simulated at steps of 11 nm mask

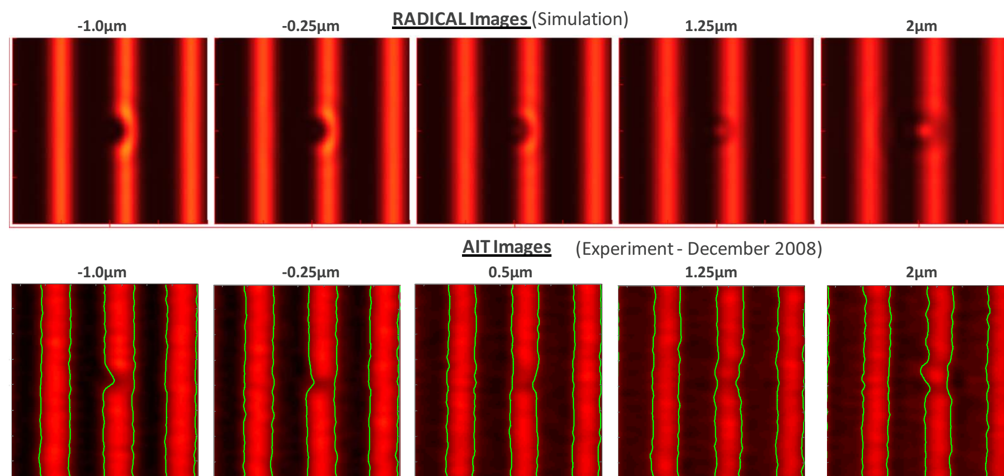

FIG. 6. (Color online) Comparison of RADICAL simulation and AIT images of a 5.3 nm tall defect centered 7 nm away from the absorber edge. The labels on each image are mask defocus.

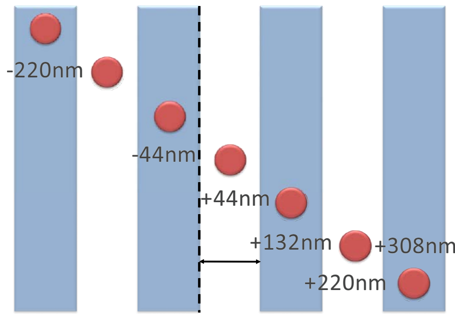

FIG. 7. (Color online) Examples of horizontal defect position range (labeled circles). The vertical dotted line shows the definition of zero-offset, and the horizontal line shows the CD that is measured in Fig. 8. All dimensions are mask scale.

scale to be sure all effects were captured. Figure 8, a plot of CD as a function of defect position relative to 88 nm lines on the mask for multiple defect sizes, summarizes the results of the simulations at best focus.

Several interesting conclusions can be drawn from these results. The first is that a 2.2 nm tall defect will cause resist bridging if it is located anywhere between 55 and 75 nm from the absorber edge. This is the worst case area in which a defect can be located. However, in practice many defects that do not cause feature bridging will still not be acceptable. For this work, a CD change of 10% due to a defect will be assumed as the maximum tolerable CD change. The RADICAL simulations in Fig. 8 show that in the worst case position, around 65 nm from the absorber line, a defect as small as 0.8 nm will cause a 10% CD change. This means if a mask blank has no defects taller than 0.8 nm, it can be relied on for 22 nm node EUV lithography, assuming there is no focus variation.

Figure 8 is not symmetric, due to the 6° incident angle of the EUV light. For negative offsets, the size of the space is actually increased by the defect and for positive offsets the space width is reduced. Also, all of the curves in Fig. 7 are shifted right due to the 6° incident angle. For normally incident light, the curves would be symmetric around an offset of +44 nm, where the defect is centered in the space. But, in Fig. 7 the curves are roughly symmetric around an offset of +66 nm, 22 nm different than the expectation for normal incidence. The absorber stack in these simulations was 87 nm tall, 75 nm of TaN, and 12 nm of an antireflection coating for mask inspection. A simple geometric ray tracing calculation of the round trip shadowing distance predicts a horizontal displacement of 18 nm from the normal incidence case. This is close to the value of 22 nm observed in simulation, suggesting that geometric approximations are a good first pass method for predicting shadowing effects. But, the most important conclusions regarding shadowing is that when considering the effect of a defect, its position and the angle of the incident light must be considered together.

C. Effect of focus on printability

Figure 9 shows a plot of CD as a function of position for three focus values. The results on this plot are similar to the results shown in Figs. 2 and 6. Basically, for positive defocus the defect becomes a bright spot and for negative defocus the defect becomes a dark spot. A dark defect near a line corresponds to a reduction in space width and a bright defect near a line causes an increase in space width. There are a few interesting cases to note in Fig. 9. The first is for a defect located at an offset of 10 nm. At best focus, this defect causes no change in CD, but at −75 nm out of focus, the defect causes nearly a 10% CD change. This means that if an inspection is done at best focus, this defect would not be detected. But, it would cause negative effects through process window. A similar situation exists for the defect at 80 nm offset. At best focus, this defect causes approximately a 10% CD change and may be acceptable at best focus. But, for even small values of defocus, it will cause a larger change and be totally unacceptable. These examples show the effects of phase defects near line and the difficulties of detecting buried defects on a patterned EUV mask.

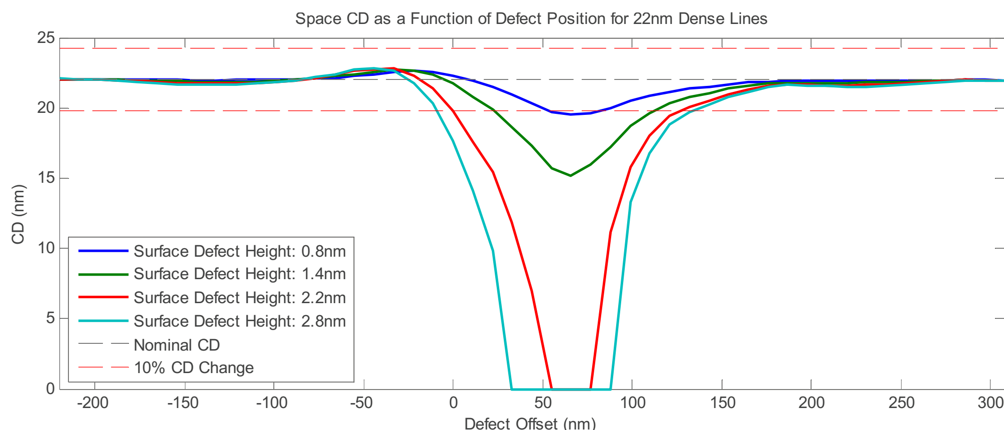

FIG. 8. (Color online) CD of 22 nm lines as a function of defect position for several surface defect heights. Offset=0 is defined as a defect centered directly on the edge of the absorber.

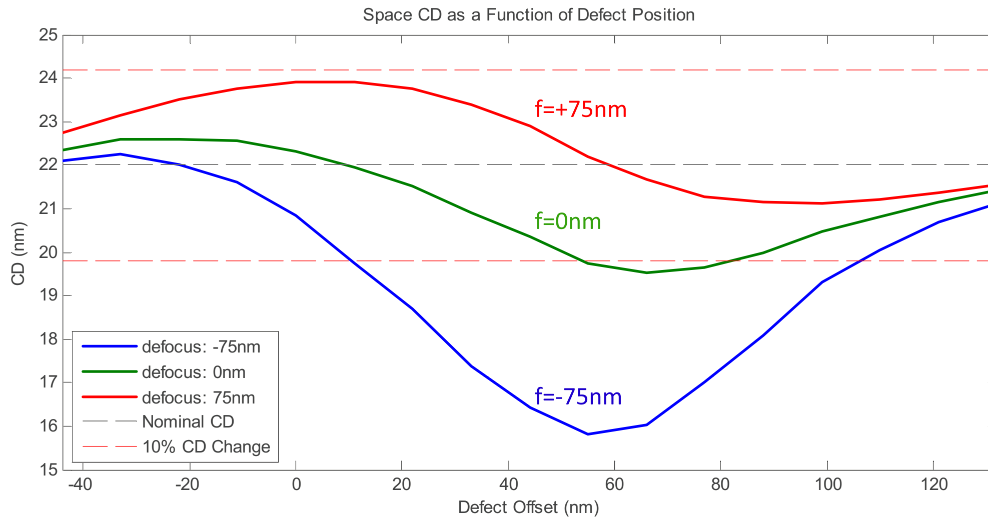

FIG. 9. (Color online) CD of 22 nm lines as a function of defect position for three focus values.

V. CONCLUSION

Buried defects in EUV masks are a significant problem for EUV lithography. Their printability is strongly dependent on their surface height, position relative to features and the level defocus. Comparisons of AIT images and RADICAL simulation confirmed the inversion of the center intensity of an isolated defect through focus and the printability of covered defects. Careful analysis of AIT images also showed that defects less than 1 nm tall will cause a noticeable CD change and can be detected by the AIT.

Simulations of 22 nm patterns show how sensitive to buried defects EUV lithography will be. A defect as short as 0.8 nm can cause a 10% CD change at best focus and will cause a greater than 10% CD change for negative focus and less than 10% CD change for positive focus. The printability of a defect is also very sensitive to its position relative to the absorber features. For 22 nm line space patterns, the worst case position is between 55 and 75 nm from the edge of the absorber when the incident light is perpendicular to the lines and causes shadowing. Also, even a covered defect may cause a CD change greater than 10%, which means a defect under the absorber cannot be ignored.

[1]Conclusion of Steering Committee at the 2008 EUVL Symposium (unpublished).
[2]K. A. Goldberg, I. Mochi, and S. Huh, Proc. SPIE **7271**, 72713N (2009).
[3]C. H. Clifford and A. R. Neureuther, J. Micro/Nanolith. MEMS MOEMS **8**, 031402 (2009).
[4]T. Liang *et al.*, J. Vac. Sci. Technol. B **25**, 2098 (2007).
[5]C. H. Clifford and A. R. Neureuther, Proc. SPIE **6921**, 692119 (2008).
[6]C. H. Clifford, S. Wiraatmadja, T. T. Chan, A. R. Neureuther, K. A. Goldberg, I. Mochi, and T. Liang, Proc. SPIE **7271**, 72711F (2009).
[7]D. G. Stearns, P. B. Mirkarimi, and E. Spiller, Thin Solid Films **446**, 37 (2004).